J. Electroanal. Chem., 71 (1976) 51—71

KINETICS OF THE HYDROGEN ELECTRODE REACTIONS ON PLATINUM IN THE $NaHSO_4$ + $KHSO_4$ EUTECTIC MELT

R.O. LEZNA, W.E. TRIACA and A.J. ARVÍA

Instituto de Investigaciones Fisicoquímicas Teóricas y Aplicadas, División Electroquímica, Universidad Nacional de La Plata, La Plata (Argentina)

(Received 29th October 1975)

ABSTRACT

The kinetics of the hydrogen electrode reactions on Pt in the $NaHSO_4$ + $KHSO_4$ melt at ca. 185° C is studied. Under potentiodynamic conditions both the anodic and cathodic processes can be interpreted with the hydrogen electrode reaction mechanism already known. At potentials more negative than 0.1 V (vs. Ag/Ag^+ (0.06 *M*)) the mechanism of the cathodic reaction changes because of a sulphide species formed on the electrode which is produced by a reduction of the melt components.

INTRODUCTION

The importance of the hydrogen electrode reaction is widely recognised either from the theoretical or the technological viewpoints. In this connection noble metals have been the most commonly studied since they are good electrocatalysts and are relatively inert over a wide range of potential even in acid electrolytes. A knowledge of the hydrogen and oxygen electrosorption characteristics on Pt which is found to be the most active of those metals, is important particularly when it refers to electrolytes such as ionic melts, where the amount of existing information is by far much less than that corresponding to aqueous solutions.

The kinetics of the hydrogen electrode in molten bisulphates was studied on various metals paying special attention to the cathodic reaction [1—5]. The kinetics of the cathodic reaction on Pt was interpreted in terms of the conventional hydrogen electrode mechanisms. According to the potential region where the reaction takes place the reaction mechanism apparently changes since the stationary Tafel slope at low overvoltages was equal to $RT/2F$ while at high overvoltages it coincided with the $2RT/F$ ratio. The two potential regions are separated by a transition region in which hysteresis occurs [5]. Recent preliminary information, however, revealed that the transition from one mechanism to another should be principally assigned to a poisoning of the electrode surface [6].

On the other hand the anodic oxidation of hydrogen in the bisulphate melts was also studied although to a much lesser extent, both on graphite [7,8], and more recently on platinum [9]. For the latter the potentiodynamic *E/I* display exhibits two anodic current peaks which resemble those reported in acid aqueous solutions at room temperature [10,11].

The present study refers to both the cathodic and the anodic processes of the hydrogen electrode in the bisulphate melt under non-stationary conditions. The data reported support the conclusions that the hydrogen electrode reaction on Pt in the bisulphate melt, within a certain potential region, fits the mechanism of reaction already known for acid aqueous solutions.

From the anodic current—potential (*I/E*) profiles obtained under adequate potentiodynamic conditions, the kinetic parameters of the partial reactions are evaluated. On the basis of these results a mechanistic interpretation of the inhibition of the cathodic reaction at high cathodic overvoltages is also given.

EXPERIMENTAL

The experimental setup is essentially the same as that reported in previous publications [2,8,12]. The electrolysis cell consisted of a conventional three electrode arrangement. The working electrode was a Pt wire (spectroscopic quality, Johnson, Matthey and Co.) of 0.5 cm^2 apparent area. Its potential was referred to a Ag/Ag^+ (0.06 *M*) electrode in the melt, which was mounted into the usual Luggin-Haber capillary tip arrangement. A Pt counter electrode properly shielded completed the electrolysis cell.

The surface of the working electrode was first mechanically polished with fine grain alumina; then, the bright surface was dipped into a 1 : 1 HNO_3 + H_2SO_4 solution, washed and dried and finally activated in the H_2 saturated melt by repetitive linear potential cycling at 100 mV s^{-1} within the potential range where a Pt oxide layer was electroformed and electroreduced. This treatment gave very reproducible results particularly when the potentiodynamic scan was limited to the potential range 0.300 to 1.05 V. This treatment was preferred for obtaining reliable kinetic data because within that potential range the hydrogen electrode equilibrium is more easily attained.

The electrolyte was prepared from 61.5% A.R. $NaHSO_4 \cdot H_2O$ (Riedel de Häen) and 38.5% A.R. $KHSO_4$ (Mallinckrodt). The mixture was dried under vacuum during several weeks at room temperature. The experiments were made at 185°C, with the melt kept under either N_2 (99.9%) or H_2 (99.99%) gas saturation.

The *I/E* curves were made under potentiostatic conditions (rise time 20 μs, potential stability ±0.1 mV). Potential sweep techniques were used as referred in previous publications [6,12,13], covering a frequency range between 10^{-3} V s^{-1} and 10^3 V s^{-1} with a maximal linearity error of 2×10^{-5} and a slope error of 2%. Potentiostatic transients with different potential steps were also recorded.

RESULTS

The rest potential

The rest potential, E_r, of a Pt electrode immersed in the bisulphate melt as well as its rate of change to attain a stable value depends on both the electrode treatment and the gas saturating the melt. Thus, for a Pt electrode, in a H_2-saturated melt, $E_r = 0.310 \pm 0.05$ V. The same electrode in contact with a N_2-saturated melt attains a less reproducible rest potential of 0.400 V.

When the electrode is anodized during 6 h at 1.050 V in a N_2-saturated melt and then the electrolysis interrupted, its potential decays slowly, reaching after 16 h a value close to 0.700 V, while in H_2 it reaches 0.310 V in about 15 min. In this case the potential decay involves a chemical reduction of the platinum oxide anodically formed and the rate of the reduction process depends on the amount of H_2 dissolved in the melt [14,15].

A Pt electrode cathodized at −0.7 V, where the H_2 evolution reaction is appreciably inhibited, and then left at open circuit in a H_2-saturated melt, also returned slowly to the rest potential of 0.310 V just mentioned.

Potentiodynamic I/E profiles run with triangular potential scans

A set of potentiodynamic *I/E* profiles run from E_r up to 1.05 V are shown in Fig. 1. The *I/E* profile under N_2 (Fig. 1a) exhibits only the double layer charging process, the anodic current peak I between 0.7 and 1.0 V which corresponds to the Pt oxide monolayer [14], and the cathodic current peak II between 0.8 and 0.4 V which is related to the electroreduction of the Pt surface [14]. The same experiment carried out under H_2 after a saturation for 2 h and with the electrode in the saturated melt for 16 h at open circuit (Fig. 1b), exhibits during the first potential scan an anodic current peak IV

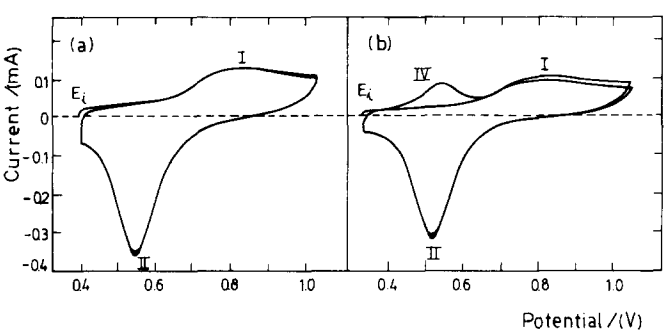

Fig. 1. Potentiodynamic *I/E* curves at $v = 0.1$ V s^{-1}; 181° C. (a) N_2 bubbling during 6 h with the electrode potential held at 1.05 V; later the cell was left at open circuit for 16 h. $E_r = 0.70$ V. (b) H_2-saturated melt; $E_r = 0.330$ V. E_i is the initial potential.

between 0.5 and 0.7 V. The profiles obtained in the following repetitive potential scans at 0.1 V s^{-1} show only the current peaks I and II. Current peak IV is always recorded under the same circumstances if the equilibrium $Pt/H_2/H^+$ is established.

These experiments show that the anodic current peak IV requires the presence of H_2 in the melt and corresponds to its electrooxidation. The amount of charge playing part in the process under the conditions prevailing in these experiments is roughly estimated as one half of that corresponding to current peak II. Furthermore, the fact that at 0.1 V s^{-1} the current peak IV is not observed during the repetitive potential scans, suggests that the time required for attaining equilibrium at the $Pt/H_2/H^+$ interface is much larger than the time spent during the potential sweep.

When the *I/E* profiles are run from 1.05 V towards the cathodic direction, extending the cathodic potential limit towards the H_2 evolution region (Fig. 2) the returning anodic scan exhibits, besides the same features already described, the appearance of another current peak III. The latter is better defined in the melt under H_2 saturation. In any circumstance the amount of charge related to the current peak IV remains practically constant. The potential shift of current peak II depends on the ageing conditions of the oxide species anodically formed on Pt as is already known [12,14]. The returning potential scan also shows at the cathodic potential extreme an activation of the Pt electrode related to the H_2 evolution reaction.

The experimental differential capacitances at the oxide free electrode surface, C_f, and at the oxide electrode surface, C_0, calculated respectively at the potentials of the ramp inversion, are assembled in Table 1. The latter are practically independent of v, the potential sweep rate, while the former decrease with it.

Potentiodynamic I/E profiles obtained with trapezoidal E/t programs

Potentiodynamic *I/E* profiles in H_2-saturated melts were initiated from 1.05 V to 0.2 V at 0.1 V s^{-1}, the electrode being held for ca. 5 min at this potential (constant cathodization time) and finally the potential scan run backwardly to 1.05 V at rates from 0.01 to 0.5 V s^{-1} (Fig. 3). They exhibit besides current peaks I, II, III and IV another cathodic current peak V, in the potential region of H_2 evolution. The height of current peak III is now larger than that of current peak IV. The heights of both anodic current peaks increase with v, as well as their height ratio which approaches unity at the largest v, as seen in the single potential sweep runs (Fig. 4). The total charge implied in the anodic process decreases rapidly with v, (Table 2), approaching a value close to 1300 μC cm^{-2} at the highest v. The contribution of the current peak III is the one which decreases quite markedly at large v.

The height of current peak III increases linearly with $v^{1/2}$ for $v < 0.6$ V s^{-1} and depends on v for $v > 0.85$ V s^{-1} (Fig. 5). As for the height of current peak IV, it approaches a linear dependence on v at $v < 1.1$ V s^{-1} (Fig. 6). It should

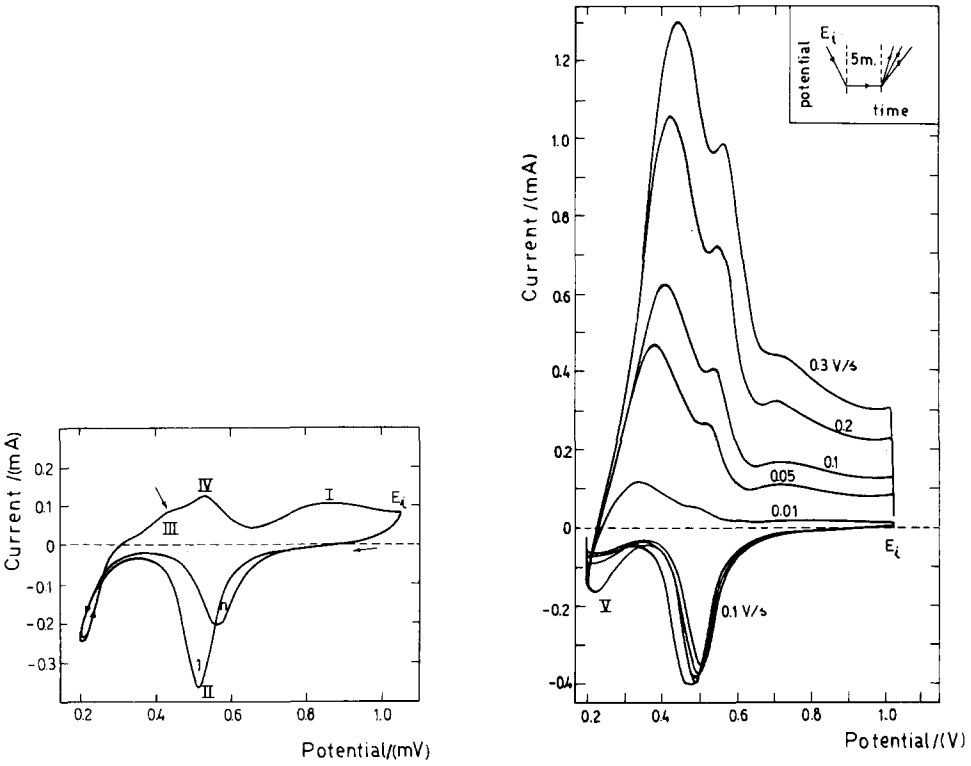

Fig. 2. Potentiodynamic I/E profiles run from E_i = 1.05 V at v = 0.1 V s^{-1}; E_r = 0.32 V; H_2-saturated melt; 185° C. The first (1) and the nth potential scans are depicted.

Fig. 3. Potentiodynamic I/E profiles run at a constant v_c and different v_a; H_2-saturated melt; 189° C. The E/time programme is indicated in the figure.

be pointed out, however, that the overlapping of the latter with current peak I and the shift of the potential of current peak IV towards anodic potentials as v increases, turn the base line for the evaluation of the height of current peak IV more uncertain as v increases beyond 1.1 V s^{-1}. Furthermore, the probable

TABLE 1

Experimental double layer capacitance at 185° C

v/mV s^{-1}	$C_f/\mu F\ cm^{-2}$	$C_0/\mu F\ cm^{-2}$
100	350	150
400	175	137
5000 [a]	93	107

[a] This result corresponds to 228° C.

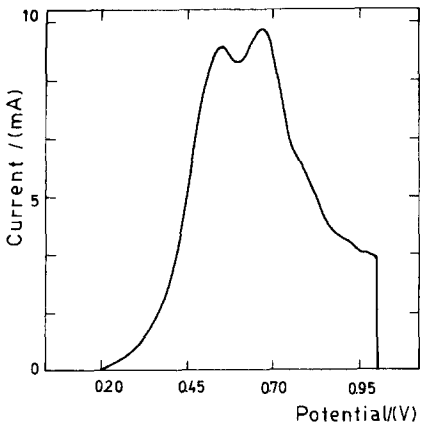

Fig. 4. Anodic I/E profile obtained under a single linear potential sweep at 6.3 V s^{-1}; H_2-saturated melt, E_r = 0.320 V, 182° C.

decrease of the amount of charge related to current peak IV with v produces a systematic deviation of the I_p vs. v plot from a straight line as v increases.

The dependences of the potentials of current peaks III and IV on v are shown respectively in Figs. 7 and 8 in terms of E_p, the current peak potential, vs. log v plots. They present the following common features: at log $v < 2.5$ there are linear E_p/log v relationships with slopes close to 2.3 RT/F. At log v comprised between 2.5 and 3.1, E_p becomes practically independent on v; finally at log $v > 3.1$ another linear E_p/log v portion is observed approaching the slope 2.3(2 RT/F).

The difference between $(E_p)_{IV}$ and $(E_p)_{III}$ decreases with v from 0.165 V to 0.107 V in the range 0.01 V $s^{-1} \leqslant v \leqslant 0.7$ V s^{-1}, but attains an average value of 0.120 ± 0.010 V in the range 0.7 V $s^{-1} \leqslant v \leqslant 7.6$ V s^{-1}.

TABLE 2

Amount of charge involved in the anodic process at different potential sweep rates

v/mV s^{-1}	Q/μC cm^{-2}
10	5895
50	5586
100	4047
500	2776
1100	2026
2000	1767
4000	1375
5000	1279
6000	1251

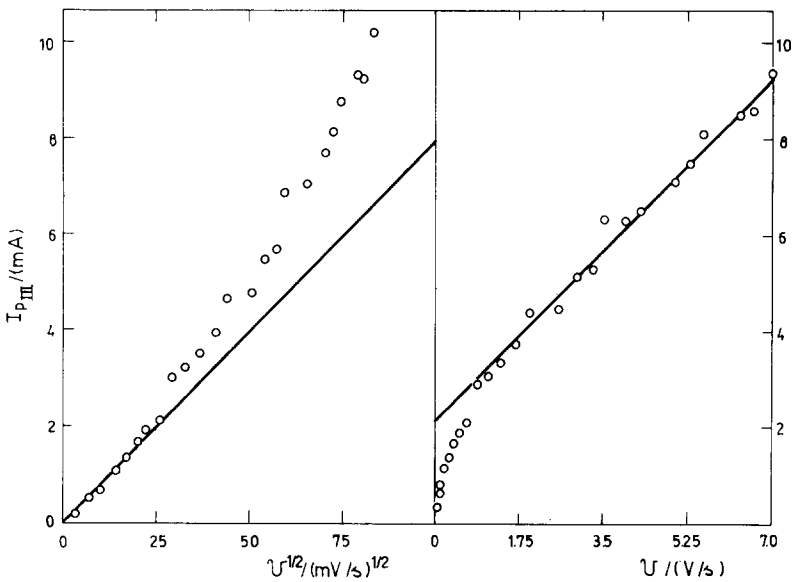

Fig. 5. Dependences of current peak (III) height on the rate of potential scan. Data taken from Figs. 3 and 4.

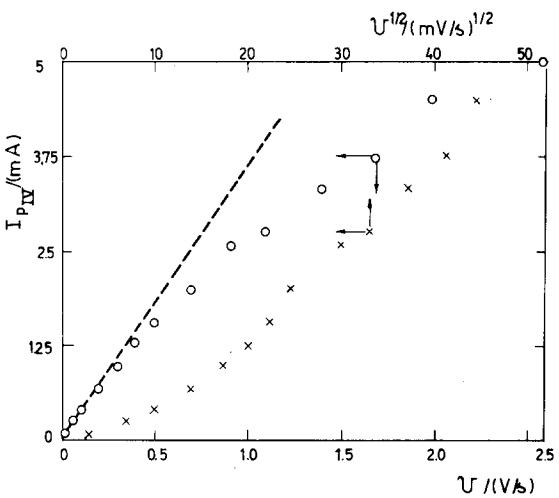

Fig. 6. Dependences of current peak (IV) height on the rate of potential scan. Data taken from Figs. 3 and 4.

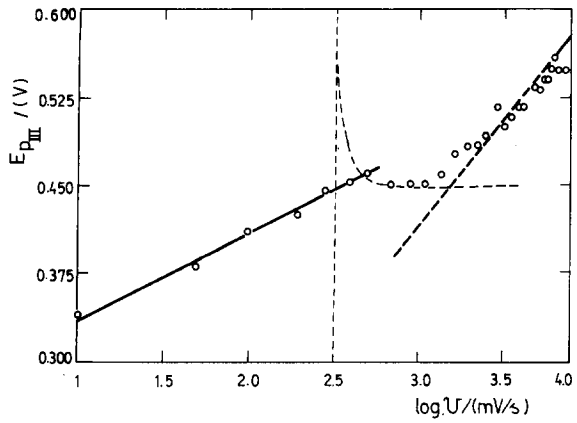

Fig. 7. Semilogarithm current peak (III) potential vs. rate of potential scan plot. Data taken from Figs. 3 and 4. Dashed lines correspond to the mechanism of reaction referred to in the discussion.

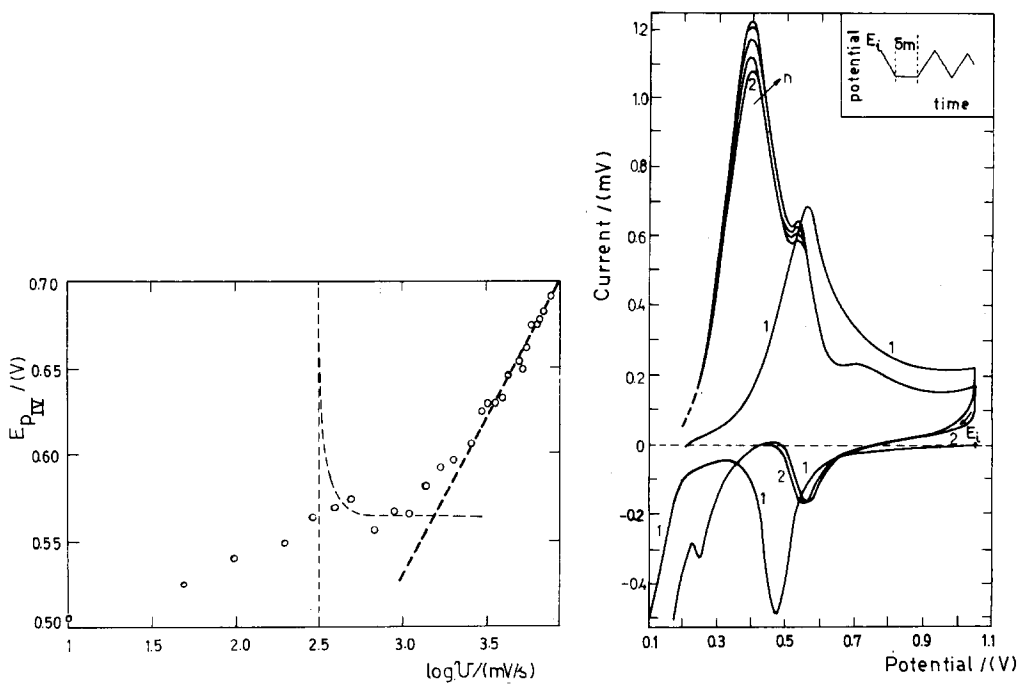

Fig. 8. Semilogarithm current peak (IV) potential/rate of potential scan plot. Data taken from Figs. 3 and 4. Dashed lines correspond to the mechanism of reaction referred to in the discussion.

Fig. 9. Repetitive *I/E* profiles run at 0.1 V s^{-1} according to the *E*/time programme shown in the figure with a cathodization at 0 V for 5 min; N_2-saturated melt; E_r = 0.355 V; 183°C.

Influence of cathodization on the I/E profiles

The *I/E* profiles shown in Fig. 9 were run as follows. After the initial single potential sweep from 1.05 V downwards, in a N_2-saturated melt, the system is potentiostatted at 0 V for 5 min. The first cathodic sweep exhibits the current peaks II and V while the first anodic scan exhibits an anodic current peak at 0.565 V, which becomes distorted at both sides by current contributions of other processes.

The repetitive second scan shows a depolarization for the H_2 evolution reaction, whose current peak V becomes now better defined. The following anodic profile changes definitely since the two anodic current peaks related to the H_2 electrooxidation are now well defined as well as current peak I. After the third potential cycle the *I/E* contours are coincident but the heights of current peaks III and IV increase. It is likely that only the actual increase in height of current peak III occurs but this also produces the apparent increase of current peak IV.

A similar experiment is made after the electrode is held during 5 min at 0.10 V (Fig. 10). The height of current peak III now decreases while its current peak potential becomes more positive during the successive potential cycling. A steady profile is attained after a large number of potential scans, but then the cathodic current peak V practically disappears.

Under repetitive triangular potential scans (Fig. 11) the H_2 electrode reaction approaches during the successive cycles a higher reversibility. It is interesting to notice that the trend of current peaks III and IV to either increase or decrease with the number of repetitive potential cycles depends on the magnitude of the cathodic potential, the cathodization time and the rate of potential sweep. When the resultant effect of these three parameters produces an accumulation of H_2 at the electrode interface, the height of those current peaks increases and the potential of current peak III becomes more cathodic (Fig. 11). The reverse situation is observed when a depletion of H_2 is produced during the successive potential cycling. Whatever the case, a stationary situation is reached after a large number of cycles.

When the experiments involve a cathodization at −0.2 V for a few minutes in a N_2-saturated melt after the first potential scan initiated at 1.05 V (Fig. 12) the following first anodic potential scans are appreciably modified both in the potential region corresponding to the electroreduction of platinum oxide and in that of the hydrogen evolution. The first cycles also exhibit current fluctuations which decrease during the following scans. After the 3rd potential scan the *I/E* contour becomes similar to those already described.

I/E profiles covering only the hydrogen evolution region

The reaction interface changes substantially when the potentiodynamic cathodization proceeds at potentials more negative than −0.1 V (Fig. 13). Thus, a Pt electrode previously potential cycled between 0.3 and 1.05 V at

0.1 V s^{-1} is a cathode more active than the one previously cathodized at —0.1 V. The latter also presents a hysteresis loop. The aspect of the Pt electrode surface after cathodizing at —0.2 V for several minutes turns out of a dull gray colour due to the formation of a sulphide layer. The latter was

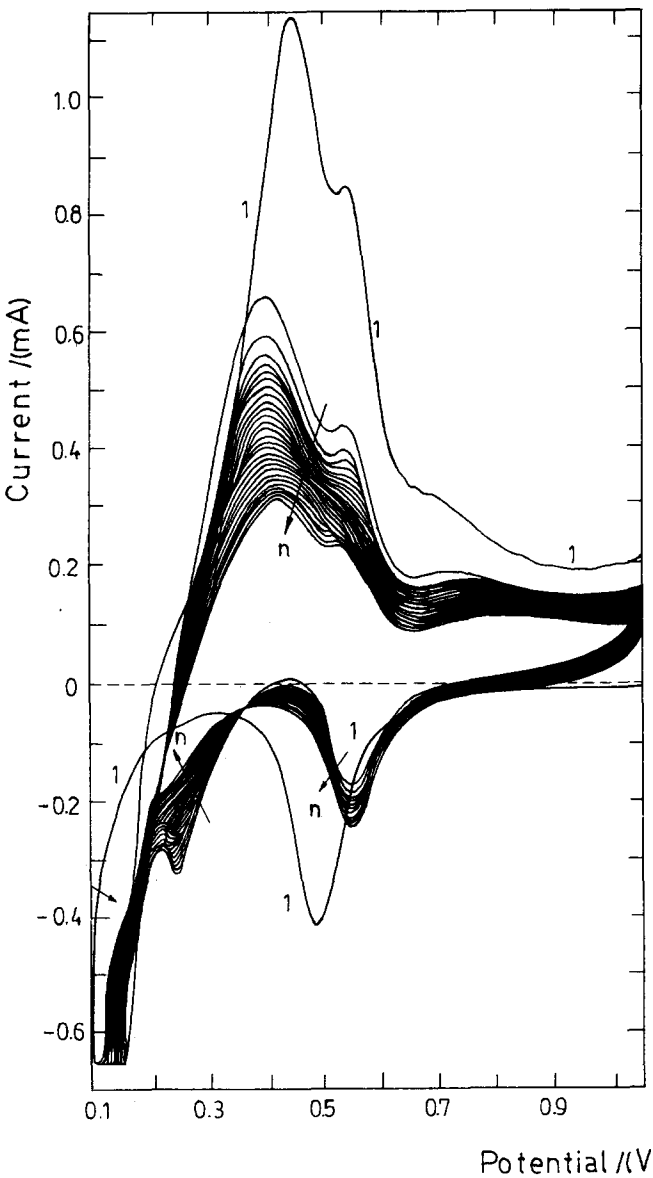

Fig. 10. Repetitive *I/E* profile run at 0.1 V s^{-1} according to the *E*/time programme shown in Fig. 9 with a cathodization at 0.1 V for 5 min; N_2-saturated melt. E_r = 0.320 V; 183°C.

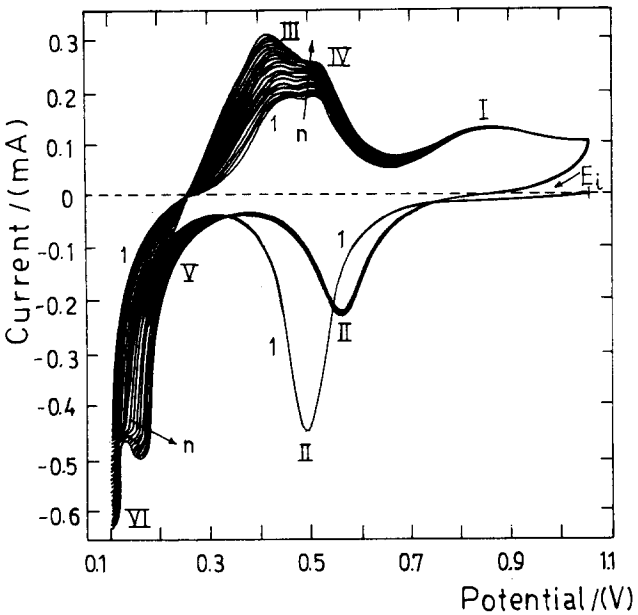

Fig. 11. Repetitive triangular potential scans at 0.1 V s^{-1}; N_2-saturated melt; E_r = 0.380 V; 183°C.

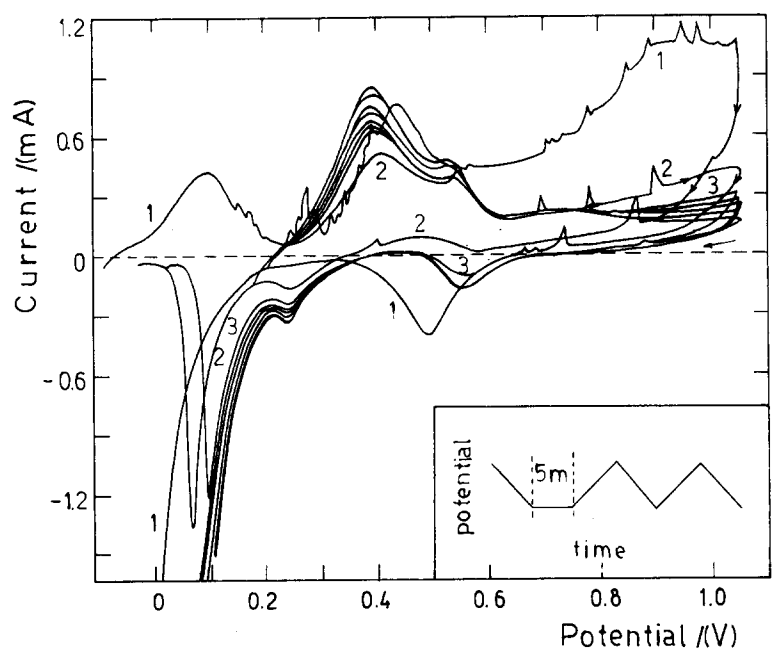

Fig. 12. Repetitive *I/E* profiles run at 0.1 V s^{-1} according to the *E*/time programme shown in the figure with a cathodization at —0.2 V for 5 min; E_r = 0.355 V; N_2-saturated melt; 183°C.

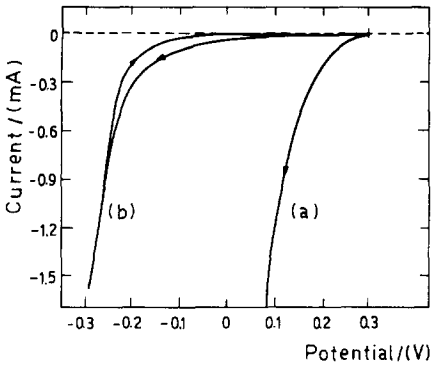

Fig. 13. Single potentiodynamic cathodic *I/E* profiles run at 0.1 V s^{-1}. (a) electrode activation by anodic potential cycling between 0.3 V and 1.05 V; (b) electrode previously cathodized at −0.1 V; 185°C.

identified through the sodium azide reaction [16]. When the cathodized electrode is left into the molten electrolyte at open circuit the sulphide layer is spontaneously removed out of the interface.

Potentiostatic I/t response of the cathodic reaction

Potentiostatic *I/t* curves are shown in Fig. 14 for the ionic melt under N_2. Initially they show the charge of the electrical double layer, then the current increases up to a maximum value at ca. 1.5 s. The amount of charge comprised between 0 and the current maximum is between 1 and 50 mC cm^{-2}, depending on the magnitude of the potential step applied. When the latter is more negative than −0.5 V, immediately after the maximum the current decays according to a I vs. t^{-1} relationship, but at $t > 2$ s a linear I vs. $t^{-1/2}$ relationship is approached (Fig. 15).

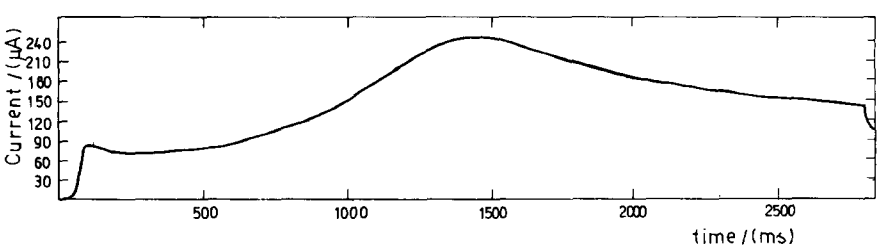

Fig. 14. Cathodic potentiostatic transient; potential step −0.12 V; N_2-saturated melt; E_r = 0.34 V; 186° C.

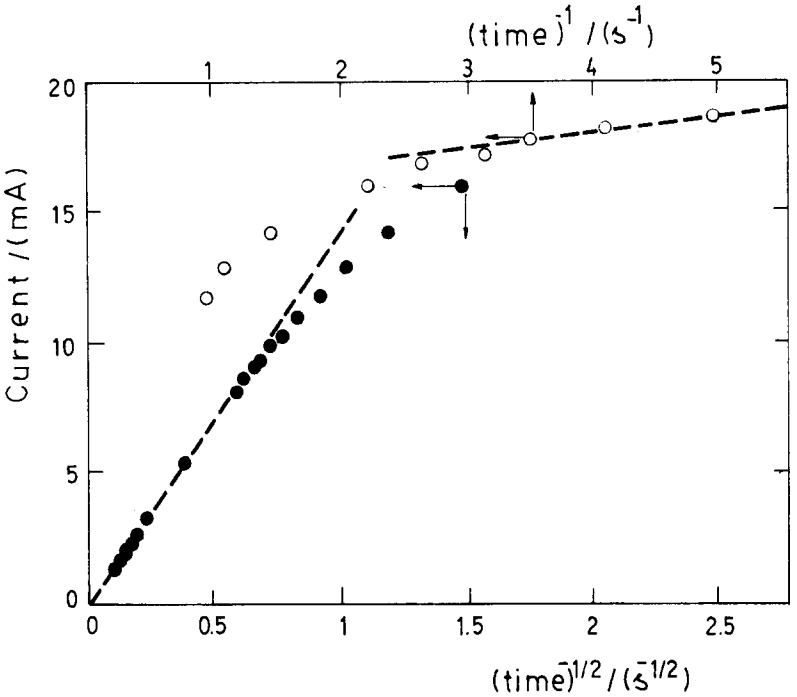

Fig. 15. Time dependences of the cathodic current under potentiostatic conditions; potential step —0.505 V; 186°C.

DISCUSSION

The electrooxidation of hydrogen

The anodic *I/E* profiles recorded with Pt electrodes in the bisulphate melt resemble those already known for the same metal in acid aqueous solutions [10,11]. Thus, the current peaks III and IV correspond to the electrooxidation of H_2 and current peak II is related to the anodic formation of the Pt surface oxide. In the bisulphate melt at 185°C, however, the potential region where the current peaks are displayed becomes narrower than that observed in aqueous solutions at room temperature. Furthermore, when the Pt electrode is properly activated the cathodic current peaks related to the hydrogen adatoms, which are complementary of the anodic ones are also observed.

The overall anodic reaction corresponding to H_2 electrooxidation is:

$$(H_2)_b \rightleftharpoons 2(H^+)_b + 2e \qquad (1)$$

and the reaction pathway to interpret it can be postulated as follows:

$$(H_2)_b \rightleftharpoons (H_2)_e \qquad (1a)$$

$$(H_2)_e + x\ Pt_\alpha + y\ Pt_\beta \rightleftharpoons x(H)Pt_\alpha + y(H)Pt_\beta \quad (1b)$$

$$(H)Pt_\alpha \rightleftharpoons (H^+)_e + Pt_\alpha + e \quad (1c)$$

$$(H)Pt_\beta \rightleftharpoons (H^+)_e + Pt_\beta + e \quad (1d)$$

$$(H^+)_e \rightleftharpoons (H^+)_b \quad (1e)$$

where: b = bulk; e = electrode; $0 \leqslant x \leqslant 2$, $0 \leqslant y \leqslant 2$ and $x + y = 2$; α and β refer respectively to weakly bound and strongly bound hydrogen adatoms on Pt. The existence of different energy sites for H_2 adsorption on Pt and other metals is frequently mentioned in the study of the gaseous H_2/metal interphases. Therefore, it is reasonable to admit at least the participation of two different energy sites on the electrode surface as earlier proposed for the adsorption of hydrogen on platinum [17—20].

Under the potentiodynamic conditions prevailing in this work, step (1a) can be considered as a simple linear diffusion of molecular H_2 from the bulk of the melt towards the reaction interface. Steps (1b) to (1d) refer to processes occurring at the reaction interface. The kinetic contribution of step (1e) should be negligible in the ionic melt under the present circumstances. The *I/E* characteristics will depend, therefore, on the relative rates v_i (i identifies the corresponding step) of the various processes, and on v, the rate of the potential perturbation. If one considers that $v_{1a} < v_{1i(i=b,c,d)}$, a kinetic contribution of step (1a) to the anodic *I/E* profile should be particularly noticed at low v. Otherwise, under a fast potential scan the only reactants are those confined at the interface at $t = 0$. One should expect, therefore, that the *I/E* voltammograms approach the two limiting cases corresponding to $v \to 0$ and to $v \to \infty$.

The anodic current peak III is only observed when a net H_2 evolution was produced by cathodization prior to running the *I/E* curve. The amount of charge involved and the current peak potential in the non-stationary process, either under a single potential scan or a repetitive potential sweep, depends upon the hydrogen concentration at the metal/electrolyte interface, as it is deduced from the influence of the cathodization time.

As v decreases, the *I/E* profile approaches an anodic limiting current due to H_2 diffusion. The polarization curve in the potential range from 0.2 to 0.4 V, can be treated as that of a quasi-stationary process. The current peak height at $v < 0.7$ V s^{-1}, approaches a linear dependence with $v^{1/2}$, but at $v > 0.7$ V s^{-1}, it attains a linear dependence with v (Fig. 5). Under a constant H_2 concentration the potential of the current peak III shows two regions of v where it changes linearly with log v (Fig. 7). The first region exhibits a slope slightly lower than 2.3 RT/F, while the slope of the second linear region, at large v, is close to $2.3(2RT/F)$.

The electrooxidation of H_2 related to current peak III, at low v is predominantly under diffusion control while at high v it becomes an activation controlled process. The latter is related to a Tafel line relationship obeyed at

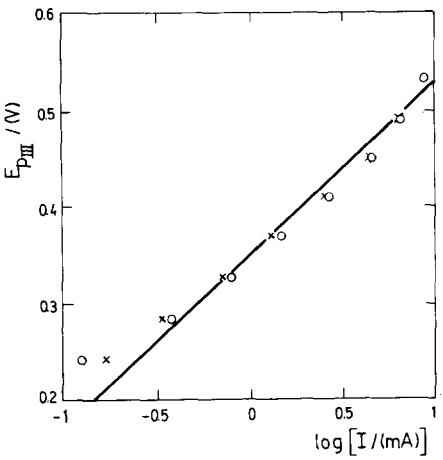

Fig. 16. Cathodic Tafel plot obtained from the initial portion of the potentiodynamic *I/E* curves at 5 V s^{-1} (×) and 7 V s^{-1} (○); 182°C.

$v > 1$ V s^{-1} by the initial portion of the anodic *I/E* profile. The corresponding apparent slope $dE/d(\log i)$ is then equal to $2.3(2RT/F)$ (Fig. 16).

The preceding analysis indicates that the kinetic information related to steps (1b—1d) can be obtained from *I/E* profiles run at $v > 1$ V s^{-1}, where any H_2 diffusion contribution should become negligible. Under these circumstances particularly when $v \to \infty$ the amount of charge involved in H_2 electrooxidation should approach that which corresponds to a monolayer of hydrogen adatoms and the kinetics of the electrode process may be controlled either by step (1c) or (1d).

The theoretical potentiodynamic *I/E* curves for such a reaction model were recently derived [21] on the assumption that there is only one kind of hydrogen adatoms on Pt. The reaction model predicts the occurrence of an anodic current peak only when the rate of the potential scan exceeds a certain limiting value, v_{lim}. At $v \gg v_{lim}$ definite current peak potential vs. v dependences are obtained depending on the rate determining step. For the irreversible process, at large v, a linear E_p vs. $\log v$ relationship is observed. The region of v where this occurs depends upon the v_{1c}/v_{1b} ratio. When step (1b) is the r.d.s., E_p is independent of v, and when v approaches v_{lim}, E_p tends to infinity. This kinetic behaviour is, in principle, observed for the oxidation of hydrogen adatoms on both Pt adsorption sites (Figs. 7 and 8). It should be pointed out that when current peak III comes out as an activation controlled process, the contribution of current peak IV becomes of the same magnitude. Current peak IV is found when the electrode is previously cathodized in the H_2 evolution region or the melt has been saturated with the H_2 gas, while current peak III appears always after previous cathodization in the H_2 evolution region. The amount of charge playing part in both current peaks, when the

contribution of H_2 diffusion becomes negligible, is of the order of that of a monolayer of hydrogen adatoms and it becomes practically independent of v (Table 2).

In spite of the extent of the electrode surface oxidation reached at 1.050 V, a comparison with data already published indicates that the amount of Pt oxide is close to a monolayer thickness [14]. Therefore, if the Pt electrode roughness factor is 1.6 [12] and the hydrogen adatom monolayer corresponds to 336 $\mu C\ cm^{-2}$, as the amount of PtO is twice this charge, the total balance, 1008 $\mu C\ cm^{-2}$, is in close agreement with the experimental limiting value. This estimation, however, is rather crude since the amount of Pt oxide formed in the absence of H_2 probably may be different of that observed in its presence. Current peak IV attains at large v a linear E_p vs. log v plot with a slope equal to $2.3(2RT/F)$. Following previous studies on H_2 electrooxidation in aqueous solutions, current peaks III and IV are assigned respectively to steps (1c) and (1d).

Taking into account the limiting conditions, namely, either the step (1b) is r.d.s. or the steps (1c)—(1d) are r.d.s., one can derive the following kinetic equations for the individual reactions [21]: At $v > 1\ V\ s^{-1}$:

$$E_p = (RT/\alpha_{1c(d)}F) \ln[\alpha F v/RT k_{1c(d)}] \tag{2}$$

where α is the anodic transfer coefficient and k_{1c}, the rate constant of step 1c. Equation (2) yields the values of α and k. The two limiting straight lines in the E_p vs. log v plot intercept at a point defined by v_i and E_p^i (see Figs. 7 and 8). Then:

$$k_{1c(d)} = (\alpha F/RT)\, v_i \exp[-(\alpha F/RT)\, E_p^i] \tag{3}$$

and

$$k_{-1c(d)} = (1-\alpha)(F/RT)\, v_i \exp[(1-\alpha)(F/RT)\, E_p^i] \tag{4}$$

Equations (3) and (4) give the values of $k_{1c(d)}$ and $k_{-1c(d)}$. Finally, from the limiting potential scan rate, v_{lim}, the limiting current density related to the adsorption of hydrogen atoms can be estimated since:

$$v_{lim} = (RT/F)\, k_1 [H_2]_e \tag{5}$$

and

$$i_{lim} = Q k_1 [H_2]_e \tag{6}$$

Q is the amount of charge required for a full coverage of the surface with a monolayer of hydrogen adatoms. Kinetic data evaluated with eqns. (2) to (6) for reaction steps (1c) and (1d) are assembled in Table 3.

It is interesting to notice that the values of α, v_{lim} and $k_{1a}[H_2]_e$ obtained from the E_p/log v plot of current peaks III and IV are coincident within the experimental errors. This indicates that a common chemical adsorption step precedes both electron transfer reactions and that the contribution of any ex-

TABLE 3

Kinetics parameters evaluated from the E_p vs. log v plots

From eqn. (2):

$\alpha_{1c} = 0.5 \pm 0.1$
$\alpha_{1d} = 0.5 \pm 0.05$
$k_{1c} = 6.7 \times 10^{-2}\ s^{-1}$
$k_{1d} = 1.3 \times 10^{-2}\ s^{-1}$

From eqn. (3):

$k_{1c} = 6.4 \times 10^{-2}\ s^{-1}$
$k_{1d} = 1.5 \times 10^{-2}\ s^{-1}$

From eqn. (4):

$k_{-1c}[H^+]_e = 6.0 \times 10^{3}\ s^{-1}$
$k_{-1d}[H^+]_e = 2.6 \times 10^{4}\ s^{-1}$

From eqn. (6):

$(v_{lim})_{III} \simeq 316\ mV\ s^{-1}$
$k_{1a}[H_2]_e = 8.1\ s^{-1}$
$(i_{lim})_{1a} = 2.7\ mA\ cm^{-2}$
$(v_{lim})_{IV} \simeq 316\ mV\ s^{-1}$
$k_{1a}[H_2]_e = 8.1\ s^{-1}$
$(i_{lim})_{1a} = 2.7\ mA\ cm^{-2}$

change reaction involving the α and β hydrogen adatoms are hardly of kinetic importance under the present circumstances. One, therefore, concludes that the *I/E* profiles related to the H_2 electrode reaction on Pt in the bisulphate melt is satisfactorily explained by the reaction mechanism involving steps (1a) to (1e).

The ratio of the amounts of charge estimated from the anodic current peaks III and IV, at $v > 1\ V\ s^{-1}$, is close to one. This suggests that the number of sites for weakly bound and for strongly bound hydrogen adatoms on Pt in the present circumstances is nearly the same. The potential difference of current peaks III and IV is about 0.120 V. This difference can be related to the free energy difference, $(\Delta G)_\alpha$ and $(\Delta G)_\beta$, between the hydrogen adatoms in the two surface states [17,18]. Thus,

$$E_{p,IV} - E_{p,III} = [(\Delta G)_\alpha - (\Delta G)_\beta]/2F \qquad (7)$$

$[(\Delta G)_\alpha - (\Delta G)_\beta]$ is ca. 6.0 kcal mol^{-1}, a figure which is smaller than the one calculated at room temperature.

The cathodic reaction

The H_2 evolution reaction on Pt in the $NaHSO_4 + KHSO_4$ melt occurs at potentials more negative than that corresponding to the electroreduction of the Pt surface oxide. The kinetics of the cathodic reaction, however, are

relatively complex and strongly depend on the potential region where it is considered. Thus, the present results clearly show that at potentials more negative than 0.3 V, the reaction takes place on an oxide free metal surface [12,14]. But the potentiodynamic data show conclusively, through the occurrence of the cathodic current peaks V and VI preceding the net H_2 evolution, that the latter takes place on a Pt surface practically covered with hydrogen adatoms. The cathodic current peak VI in the acid melt is less clearly defined than that observed in the acid aqueous media [10,11]. Most of the cathodic *I/E* profiles exhibit current peak VI as a small hump (see, for instance, Figs. 10 and 11 at the cathodic potential extremes). These current peaks as earlier suggested should also be related to two energetically different H—Pt bonds [17—20].

On the other hand, at potentials more negative than 0.1 V an inhibiting effect begins to be noticed on the cathodic reaction. This effect is caused by products likely formed by a chemical reduction of the melt at the interface by hydrogen adatoms. For the sake of simplicity, the following discussion of the cathodic reaction will be independently considered in both potential regions.

(a) The reaction on the oxide free electrode. Under these circumstances the rest potential is related to the equilibrium potential of the H_2 electrode in the melt. The kinetic characteristics of the cathodic reaction on the platinum oxide free electrode previously activated by repetitive potential cycling are comparable to those already reported for the reaction taking place on platinized platinum under stationary conditions [3], where the cathodic Tafel slope is equal to $2.303(RT/2F)$ V/decade. From the present data the calculation of the exchange current density, i_0, can be made from the linearized portions of the anodic and cathodic *I/E* profiles a few mV apart from the equilibrium potential. Thus, $dE/dI = RT\nu/nFI_0$, where ν is the stoichiometric number ($\nu = 1$ for the desorption step as r.d.s.). Values of i_0 depend on the H_2 pressure at the interface. The latter can be evaluated from the Nernst equation obeyed by the potential of the current peak III at low v, where the constant of the equation, $(E_p)_{III}(P_{H_2} = 1 \text{ atm})$ is extrapolated from the $(E_p)_m$ vs. n_s^{-1} plot, for $n_s \to \infty$ (n_s is the number of potential scans for a set of repetitive *I/E* profiles yielding a H_2 accumulation during potential cycling). The values of i_0 depend linearly on $(P_{H_2})^{1/2}$ (Fig. 17) as has been already observed [7,8]. The i_0 value at $P_{H_2} = 1$ is in good correspondence with the one previously reported [7].

These results, therefore, are consistent with the H_2 electrode reaction mechanism already discussed particularly for the anodic process. The rate of the cathodic reaction is, thus, determined by the desorption of hydrogen adatoms [3].

(b) The cathodic reaction on a poisoned Pt electrode. The cathodic passivation is related to the formation of a sulphide species at the reaction interface.

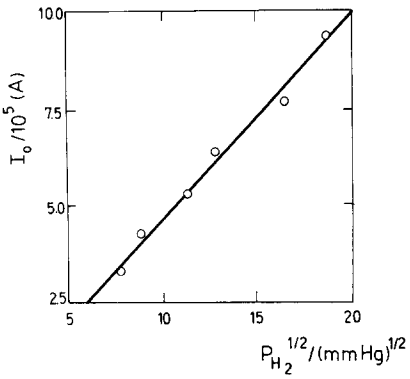

Fig. 17. Dependence of i_0 on the hydrogen pressure; 180°C.

Under these circumstances the H_2 evolution reaction is appreciably hindered and the cathodic Tafel constant under quasi-steady conditions attains the ratio $2.3(2RT/F)$ previously reported [2]. The kinetic changes of the H_2 electrode reaction due to the interference of the sulphide species can be interpreted through the I/time relationship derived from the potential step experiments, when the potential step exceeded 0.5 V. Those transients approach two limiting laws depending on the time scale considered. The I vs. t^{-1} relationship suggests that the current is under adsorption kinetics, following the Elovich kinetic isotherm for a uniformly homogeneous surface, as recently described for the adsorption of sulphur and simple organic substances on Pt [22—24]. The instantaneous current is then given by:

$$I = Q/\gamma f t \tag{8}$$

Q is the charge passed through the interface during the adsorption process up to total coverage of the surface; γ is a constant and f is the inhomogeneity coefficient of the electrode surface.

The second limiting case, satisfactorily approached as $t \to \infty$, suggests that the reaction becomes a diffusion controlled process [22].

The likely mechanism of reaction for the inhibited electrode must involve a reactant initially present at the interface, which is likely to be electroreduced by hydrogen adatoms yielding the sulphide species. The latter, probably electrosorbed on the Pt surface, produces a strong decrease of the hydrogen adatoms concentration biasing, thus, the H_2 discharge reaction.

The initial reactant for this process presumably is SO_3, which exists through the following equilibrium:

$$2HSO_4^- \rightleftharpoons SO_3 + SO_4^{2-} + H_2O \rightleftharpoons S_2O_7^{2-} + H_2O \tag{9}$$

The following complex reaction scheme involving a set of consecutive and

parallel steps are considered:

$$Pt + H^+ + e = HPt \quad (10)$$

$$2PtH = H_2 + 2Pt \quad (11a)$$

$$SO_3(bulk) = SO_3(interface) \quad (11b1)$$

$$SO_3(interface) + 2PtH = SO_2(interface) + H_2O + 2Pt \quad (11b2)$$

$$SO_2(interface) = SO_2(solution) \quad (11b3)$$

$$SO_2(interface) + 6PtH = 2H^+ + S^{2-}(interface) + 2H_2O + 6Pt \quad (11c1)$$

$$Pt + S^{2-}(interface) = Pt(S^{2-}) \quad (11c2)$$

Reaction (11b2) interferes directly with the rate determining step of the H_2 evolution reaction. The overall effect of SO_3 electroreduction is to block the electrode surface for hydrogen adsorption and consequently the rate of the second order r.d.s. should decrease quite markedly. During the potentiostatic transient there is first an accumulation of hydrogen adatoms up to the maximum current. Immediately afterwards, the current decreases due to processes (11b1) to (11c2) which, during this intermediate transient period becomes an adsorption controlled reaction. Finally, at large t, due to the depletion of SO_3 at the interface the process becomes diffusion controlled. The electrode, initially predominantly covered by H adatoms, becomes at the end a poisoned electrode offering a different reaction surface for the H_2 evolution reaction.

The interference of reactions (11b1)—(11c2) in the H_2 evolution reaction explains the change of the cathodic Tafel slope from $2.3(RT/2F)$ to $2.3(2RT/F)$ by an inhibition of the desorption of hydrogen adatoms. When the active electrode sites become blocked by the sulphide species, the rate of the controlling step could attain a value so low that an alternative reaction step operates. Under these circumstances it is likely that the initial electron transfer step becomes the r.d.s.

The poisoning of the heterogeneous hydrogen adatom desorption by H_2S is already known for Fe and Ni [25]. Furthermore, the H_2 discharge on Pt in concentrated H_2SO_4 is also influenced in a similar manner because of a complex reduction of the acid itself [26,27]. The effect of the adsorbed species naturally reflects through the whole I/E profile, including the formation and reduction of the Pt oxide layer [28]. The cleaning of the poisoned electrode can also be achieved during the potential cycling but the corresponding reactions are at present not definitely established.

ACKNOWLEDGEMENT

This work is part of the research program of the Electrochemistry Division of INIFTA, sponsored by the Universidad Nacional de La Plata, the Consejo

Nacional de Investigaciones Científicas y Técnicas of Argentina and the Comisión de Investigaciones Científicas de la Pcia. de Bs As.

REFERENCES

1 A.M. Shams El Din, Electrochim. Acta, 7 (1962) 613.
2 H.A. Videla and A.J. Arvía, Electrochim. Acta, 10 (1965) 21.
3 A.J. Arvía, A.J. Calandra and H.A. Videla, Electrochim. Acta, 10 (1965) 33.
4 A.J. Arvía, A.J. Calandra and H.A. Videla, Anales Asoc. Quím. Arg., 54 (1966) 143.
5 D. Gilroy, Electrochim. Acta, 17 (1972) 1771.
6 R.O. Lezna, W.E. Triaca and A.J. Arvía, J. Electroanal. Chem., 57 (1974) 113.
7 E.J. Balskus, J.J, Podestá and A.J. Arvía, Electrochim. Acta, 16 (1971) 1663.
8 E.J. Balskus, W.E. Triaca and A.J. Arvía, Electrochim. Acta, 17 (1972) 45.
9 H. Urtizberea, A.J. Calandra and A.J. Arvía, J. Electroanal. Chem., 55 (1974) 145.
10 K. Vetter, Electrochemical Kinetics, Academic Press, New York, 1967, p. 549.
11 M.W. Breiter, Electrochemical Processes in Fuel Cells, Springer, Berlin, 1969, p. 48.
12 N.R. de Tacconi, A.J. Calandra and A.J. Arvía, J. Electroanal. Chem., 51 (1974) 25.
13 G. Paus, A.J. Calandra and A.J. Arvía, Anales Soc. Cient. Arg., 192 (1971) 35.
14 N.R. de Tacconi, A.J. Calandra and A.J. Arvía, J. Electroanal. Chem., 49 (1974) 145.
15 S. Schuldiner, M. Rosen, D.R. Flinn and C.H. Presbrey, Jr., Electrochim. Acta, 17 (1972) 1637.
16 F. Feigl, Spot Tests, Elsevier, Amsterdam, 1954.
17 M.W. Breiter, J. Electroanal. Chem., 8 (1964) 449.
18 M.W. Breiter, Trans. Faraday Soc., 62 (1966) 2887.
19 H. Kita, J. Res. Inst. Catalysis Hokkaido Univ., 17 (1969) 77.
20 J. Horiuti and T. Toya in M. Green (Ed.), Solid State Surface, Vol. 1, Marcel Dekker, New York, 1969, pp. 1—86.
21 A.M. Alquié-Redon, A. Aldaz and C. Lamy, J. Electroanal. Chem., 52 (1974) 11.
22 T. Loucka, J. Electroanal. Chem., 36 (1972) 369.
23 T. Loucka, J. Electroanal. Chem., 36 (1972) 355.
24 T. Loucka, J. Electroanal. Chem., 36 (1972) 319.
25 I. Katajczykowa, Bull. Acad. Polon. Sci., 17 (1969) 693.
26 H.A. Garrera, J.S.W. Carrozza and A.J. Arvía, Electrochim. Acta, 13 (1968) 771.
27 H.A. Garrera, J.S.W. Carrozza and A.J. Arvía, Electrochim. Acta, 14 (1969) 205.
28 T. Loucka, J. Electroanal. Chem., 44 (1973) 221.